IOP Publishing Phys. Biol. 14 (2017) 066001 https://doi.org/10.1088/1478-3975/aa90ea

Physical Biology

PAPER

RECEIVED
27 May 2017

REVISED
14 September 2017

ACCEPTED FOR PUBLICATION
4 October 2017

PUBLISHED
16 November 2017

# Exciton transport in the PE545 complex: insight from atomistic QM/MM-based quantum master equations and elastic network models

**Sima Pouyandeh[1,2,3], Stefano Iubini[3,4], Sandro Jurinovich[5], Yasser Omar[1,2], Benedetta Mennucci[5] and Francesco Piazza[3,6]**

[1] Instituto de Telecomunicações, Physics of Information and Quantum Technologies Group, Portugal
[2] Instituto Superior Técnico, Universidade de Lisboa, Portugal
[3] Centre de Biophysique Moléculaire, (CBM), CNRS UPR 4301, Rue C. Sadron, 45071, Orléans, France
[4] Dipartimento di Fisica, Università di Firenze and INFN, Sezione di Firenze, Via G. Sansone 1, 50019 Sesto F.no (FI), Italy
[5] Dipartimento di Chimica e Chimica Industriale, University of Pisa, via G. Moruzzi 13, 56124 Pisa, Italy
[6] Université d'Orléans, Château de la Source, F-45071 Orléans Cedex, France

**E-mail:** Francesco.Piazza@cnrs-orleans.fr

**Keywords:** quantum master equations, PE545 complex, bilins, elastic network models

Supplementary material for this article is available online

## Abstract

In this paper, we work out a parameterization of environmental noise within the Haken–Strobl–Reinenker (HSR) model for the PE545 light-harvesting complex, based on atomic-level quantum mechanics/molecular mechanics (QM/MM) simulations. We use this approach to investigate the role of various auto- and cross-correlations in the HSR noise tensor, confirming that site-energy autocorrelations (pure dephasing) terms dominate the noise-induced exciton mobility enhancement, followed by site energy-coupling cross-correlations for specific triplets of pigments. Interestingly, several cross-correlations of the latter kind, together with coupling–coupling cross-correlations, display clear low-frequency signatures in their spectral densities in the 30–70 $cm^{-1}$ region. These slow components lie at the limits of validity of the HSR approach, which requires that environmental fluctuations be faster than typical exciton transfer time scales. We show that a simple coarse-grained elastic-network-model (ENM) analysis of the PE545 protein naturally spotlights collective normal modes in this frequency range that represent specific concerted motions of the subnetwork of cysteines covalenty linked to the pigments. This analysis strongly suggests that protein scaffolds in light-harvesting complexes are able to express specific collective, low-frequency normal modes providing a fold-rooted blueprint of exciton transport pathways. We speculate that ENM-based mixed quantum classical methods, such as Ehrenfest dynamics, might be promising tools to disentangle the fundamental designing principles of these dynamical processes in natural and artificial light-harvesting structures.

## 1. Introduction

Environmental effects can strongly influence the dynamics of quantum excitations in complex media. In the context of photosynthetic complexes [1, 2], a crucial role is played by the ultrafast process that allows the transfer of energy, absorbed from photons by pigments, to the reaction center during the early stages of photosynthesis. In this respect, one of the most relevant issues concerns the mechanisms that allow a fast and efficient energy transfer within the complex. The presence of a noisy protein scaffold that encompasses the pigment network represents an essential feature of the problem. Indeed, at the microscopic level, chromophores experience environmental vibrations [3] that produce fluctuations of the local pigment site-energies and pigment–pigment couplings. Additionally, very slow protein motions contribute by adding static disorder to the unperturbed exciton dynamics.

One of the key findings of recent theoretical research is that in certain regimes noise can act as a positive factor for transport efficiency. In particular, it has been shown [4–6] that exciton transfer efficiency can be enhanced by pure dephasing noise, which accounts for site-energy fluctuations due to protein vibrations. Optimal transport efficiency was found for intermediate amplitudes of the noise strength, in a region of the parameters compatible with room temperature condi-

tions. The reason why a certain amount of dephasing is beneficial is that external fluctuations may promote excitonic transitions that speed up the global transfer process.

Understanding the role of environmental effects on the exciton dynamics necessarily requires a microscopic description of the environment-induced fluctuations on the electronic degrees of freedom. Extensive studies [3, 7–10] have been performed in order to understand the role of spatio-temporal noise correlations in site-energy fluctuations and the presence of specific vibrational modes that interact with the electronic ones. Although in photosynthetic systems site-energy fluctuations are considerably larger than fluctuations in the site–site coupling energies [11, 12], it has been shown by Silbey *et al* [13, 14] that even small, correlated coupling fluctuations may have a deep impact in speeding up the energy transfer process. Moreover, it was found that nonvanishing correlations between site-energy and coupling fluctuations may strongly enhance or suppress long-lived oscillations in populations, depending on the sign of the correlation. These effects were initially studied within a generalized Haken–Strobl–Reineker (HSR) model [15, 16], where external environmental fluctuations are described in terms of classical Gaussian Markov processes (white noise). Further studies by Huo and Coker [17] performed with refined numerical techniques [18] along with more recent ones by other groups [19–21], using various modified quantum master equation (QME) approaches, showed that the same phenomenology also persists with explicit non-Markovian harmonic models of heat bath.

In this paper, we focus on the dynamics of the phycoerythrin 545 (PE545) light-harvesting complex of the marine cryptophyte alga *Rhodomonas sp.* strain CS24, that comprises eight bilins [22–25], see figure 1. This system absorbs incident sunlight very efficiently. Interestingly, recent studies have ascribed this efficiency to the structural flexibility of the pigments, which allows the modulation of their absorption energy through local pigment-protein interactions [12]. This light-harvesting system seems to work as a *funnel*, driving the excitons formed in the core of the complex—i.e. at the two strongly coupled PEB 50/61 pigments (see figure 1)—to the surface. This in turn is believed to facilitate the transfer of the excitonic energy to another complex in the neighborhood, or to the reaction center, where the charge separation process may occur [12]. Even more interestingly, in a recent paper, some of the present authors have shown that the spectral densities of individual pigments of PE545 may be very different with respect to those averaged over pseudo-symmetric pairs or over all pigments [26]. This strongly warns against any uniform parameterization of excessively simplistic quantum master equation approaches, such as [4], where a single dephasing rate is assumed to describe the whole extent of possible correlations. Rather, the need for a proper *ab initio* parameterization of QME-based methods is apparent, as it is the whole range of possible correlations (site-energy/site-energy, coupling/coupling and site-energy/coupling) that appears to contain the fine details of phonon-mediated exciton transport in light-harvesting proteins.

The aim of this paper is to clarify the role and the relative weight of the different types of correlation among fluctuations, involving both site energies and coupling strengths, by parametrizing a general HSR quantum master equation directly from atomistic quantum-mechanics/molecular-mechanics (QM/MM) simulations with atomic-level classical description of the protein environment. In section 2, we describe this procedure with the aim of computing the transport parameters of the complex at room temperature and study their dependence on the strength of the environment-induced perturbations. Accordingly, in section 3 we show that the so-called Zeno regime [4, 27], corresponding to a drop in exciton transfer efficiency at high noise strength, is suppressed by coupling fluctuations at high temperature. However, while the Zeno regime might be relevant for some materials, as has already been shown by some of the present authors [28], it is certainly *de facto* inaccessible to biological macromolecules, as the protein scaffolds would fall apart well before reaching such high temperatures. From a theoretical standpoint, we show that the theoretical suppression of the Zeno effect can be simply interpreted in terms of the emergence of a classical random walk for the exciton dynamics. In this limit, we show that the quantum master equation becomes a simple classical Fokker–Planck equation, whose diffusivity tensor is given by the coupling–coupling correlation matrix. Furthermore, in section 3 we show that slow frequency components at the limits of validity of the HSR approach are present in specific cross-correlations. In section 4 we use an original elastic network model approach to rationalize the emergence of these low frequencies in terms of specific collective modes preferentially involving the subnetwork of cysteines that are covalently linked to the pigments. In section 5 we summarize our results, critically discussing HSR based approaches, and suggesting an alternative way to dissect the fold-rooted spatiotemporal signatures of exciton transport in light-harvesting structures based on elastic network models.

## 2. Reduced quantum master equation from QM/MM simulations

We consider a many-body representation of the light-harvesting complex with $N = 8$ pigments in the presence of a single exciton, described by the following tight-binding Hamiltonian:

$$H_0 = \sum_{m=0}^{N-1} \epsilon_m |m\rangle\langle m| + \sum_{n<m}^{N-1} J_{mn}\Big(|m\rangle\langle n| + |n\rangle\langle m|\Big) \quad (1)$$

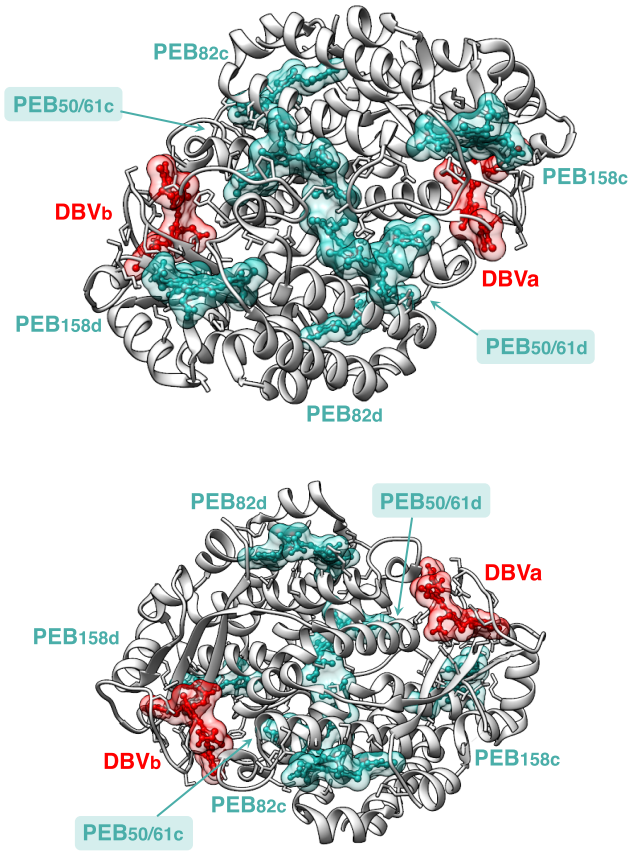


**Figure 1.** The structure of the PE545 light-harvesting complex (dimer) with the eight light-absorbing pigments (bilins) shown explicitly. There are two types of bilins in the complex: dihydrobiliverdins (DBV) and phycoerythrobilins (PEB). Both are linear molecules consisting of four pyrrole rings (tetrapyrroles). All the eight pigments are covalently linked to the protein scaffold by relatively stable thioether bonds involving specific Cysteines in the protein matrix [29]. The central pair of highly correlated PEB pigments is highlighted. Top: front view with the PEB50/61 pair in the front. Bottom: rear view with the PEB50/61 pair in the back.

where the state $|m\rangle$ denotes an electronic excitation localized on chromophore $m$. The site energies and pigment–pigment couplings are given by $\epsilon_m$ and $J_{mn}$ respectively. For the parametrization of the Hamiltonian $H_0$ of the bilin system we refer to [12]—see also the online supporting information (stacks.iop.org/PB/14/066001/mmedia). The associated network is shown in figure 2, where we identify the nodes of the network from $m = 0$ to $m = N - 1 = 7$ with the eight bilin molecules of the complex and (weighted) links represent the associated coupling strengths. To include the effect of a thermally fluctuating environment, the original approach of Haken and Strobl [15, 16] requires one to solve a modified problem, described by the Hamiltonian

$$H(t) = H_0 + h(t) \tag{2}$$

where the Hermitian operator $h(t)$ is a time-dependent perturbation of the Hamiltonian $H_0$, whose temporal evolution reflects the bath dynamics. In this framework, the so called Haken–Strobl–Reineker model [14, 16] assumes that the environmental fluctuations $h(t)$ are classical Gaussian Markovian processes with zero average and correlations given by

$$C_{mnpq}(t - t') \equiv \langle h_{mn}(t) h_{pq}(t') \rangle = 2\delta(t - t')\Gamma_{mnpq} \tag{3}$$

where the four-indices tensor $\Gamma_{mnpq}$ is invariant under the following set of index permutations [14]

$$(mn) \to (nm) \quad (pq) \to (qp) \quad (mnpq) \to (pqmn). \tag{4}$$

With the above hypotheses, the information on the external environment is fully encoded in the tensor $\Gamma_{mnpq}$.

Finally, to account for the exciton losses due to internal recombination processes and exciton transfer to the reaction center, we add to the system Hamiltonian $H_0$ an anti-Hermitian operator [4, 14, 30] defined as

$$\mathrm{i}H_d = -\mathrm{i}\hbar \sum_m (\alpha_m + \kappa_m)|m\rangle\langle m|. \tag{5}$$

In the above formula, $\alpha_m$ and $\kappa_m$ are the site-dependent recombination and trapping rates, respectively. Altogether, it can be shown [16] that the evolution of the density matrix of the system is described by the following master equation

$$\frac{\mathrm{d}\rho_{nm}}{\mathrm{d}t} = -\mathrm{i}\,[H_0, \rho]_{nm} - \mathrm{i}\,[H_d, \rho]^+_{nm} + \sum_{pq} \left(2\Gamma_{npqm}\rho_{pq} - \Gamma_{nppq}\rho_{qm} - \Gamma_{pmqp}\rho_{nq}\right) \tag{6}$$

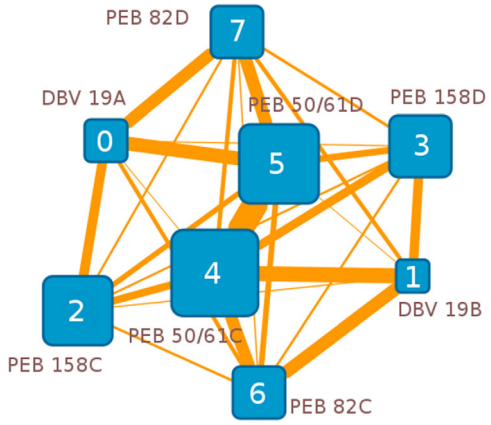


**Figure 2.** The exciton network corresponding to the Hamiltonian $H$ of the PE545 light-harvesting antenna according to the parameters reported in [12]. The sizes of nodes and edges account for the amplitude of average pigment site-energies and couplings, respectively. The spatial arrangement of nodes reflects the position of chromophores in the complex, see figure 1, rear view. In particular, the two central PEBs (50/61) appear clearly to form the most *connected* pair in the system.

where the symbols $[\cdot,\cdot]$ and $[\cdot,\cdot]^+$ denote the commutator and the anti-commutator respectively. The first term in the r.h.s. of equation (6) describes the unitary part of the evolution, the second incorporates the dissipative effects defined in equation (5), while the third accounts for the action of the incoherent noise.

Following Vlaming and Silbey [14], it is instructive to single out three physically different types of elements of the tensor $\Gamma$:

(i) Site energy-site energy correlations, $\Gamma_{mmnn}$;
(ii) Site energy-coupling correlations, $\Gamma_{mmpq}$ with $p \neq q$;
(iii) Coupling–coupling correlations, $\Gamma_{nmpq}$ with $n \neq m$ and $p \neq q$.

In the following subsection, we will discuss how to estimate the bath tensor $\Gamma$ directly from atomic-level QM/MM simulations.

### 2.1. Microscopic description of the exciton environment

All the excitonic parameters (site energies and excitonic couplings in $H(t)$, see equation (2)) have been calculated with a polarizable quantum mechanical/molecular mechanical (QM/MMPol) methodology [31] using a trajectory obtained with a ground-state classical MD simulation of PE545 in water (see [22] for more details). In particular, we extracted 60 000 snapshots every 5 fs, corresponding to 300 ps of a MD simulation of PE545 for the subsequent QM/MMPol calculations. Because of the considerable computational cost involved in the QM/MMPol calculations, we adopted the ZINDO semi-empirical method [32] to describe the excited states of the pigments, whereas the protein and the solvent were described using a polarizable force field. All details about the QM/MMPol model are reported in [12] and [22]. A detailed study on the parametrization of $H_0$ for PE545 is contained in [12].

Concerning the environmental fluctuations described by the term $h(t)$, the white noise approximation of the HSR model, equation (3), assumes that the bath degrees of freedom decorrelate much faster than the typical exciton timescales. Therefore, in this limit, one can formally integrate equation (3), writing

$$2\Gamma_{mnpq} = \int_{-\infty}^{+\infty} C_{mnpq}(\tau)\,\mathrm{d}\tau \qquad (7)$$

where it clearly appears that $\Gamma_{mnpq}$ are related to the zero-frequency limit of the Fourier transform $C_{mnpq}(\omega)$. Notice that, despite the integration up to arbitrarily large times in the above formula, the relevant contribution of correlations to the tensor $\Gamma$ is expected to come exclusively from very short times. An instructive example is offered by the case of an exponential decay of the correlation function, $C(\tau) = 2C(0)\exp(-|\tau|/\tau_c)$, which gives $\Gamma = C(0)\tau_c$. In this example, $\tau_c$ defines the characteristic timescale of bath correlations, so that the contribution to the integral in equation (7) for times $|\tau| \gg \tau_c$ is exponentially small in $\tau$. A direct calculation of the tensor $\Gamma_{mnpq}$ from equation (7) would implicitly overlook the existence of any finite timescale for the environment degrees of freedom. Therefore, for the HSR approximation to hold, it is necessary to compare the typical environmental correlation times with the intrinsic exciton timescales. In the simplest hypothesis of a single time decay constant, we replace equation (3) with

$$C_{mnpq}(t-t') \equiv \langle h_{mn}(t)h_{pq}(t')\rangle = \frac{2\mathrm{e}^{-|t-t'|/\tau_{mnpq}}}{\tau_{mnpq}}\Gamma_{mnpq}. \qquad (8)$$

For our purposes, this assumption provides a good representation of the low-frequency part of the associated spectral density. Indeed, we have verified that more detailed descriptions consisting of biexponential or multi-exponential decays [33] do not significantly change our results. Accordingly, an estimate of the spectral width $\omega_{mnpq} = 2\pi/\tau_{mnpq}$ and of the amplitude $\Gamma_{mnpq}$ is obtained from the QM/MM data by consistently fitting a Lorentzian distribution to the cosine Fourier transform of the correlation function in (8) defined as

$$C_{mnpq}(\omega) = \int_0^{\infty} C_{mnpq}(t)\,\cos(\omega t)\,\mathrm{d}t \qquad (9)$$

(see the supplemental material for further details). An effective infrared threshold $\Theta$ is introduced, in order to exclude the contribution of slow environmental correlations which are inconsistent with the HSR white-noise approximation of the exciton-protein coupling dynamics. Specifically, in equation (8) we have neglected the coupling coefficients $\Gamma_{mnpq}$ displaying a decaying time $\tau_{mnpq} > \Theta$. For the choice

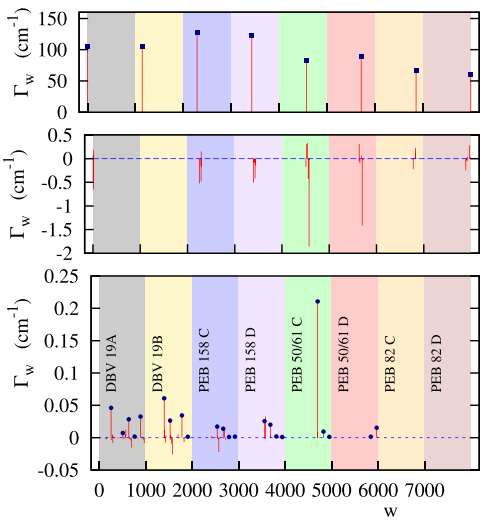


**Figure 3.** Bath parameter $\Gamma_w$ extracted from QM/MM simulations at $T = 300K$. The index $w$ is the octal representation of the number $mnpq$. Upper panel: site energy autocorrelation terms of type $\Gamma_{mmmm}$ (sector $i$); central panel: site energy-couplings correlations of type $\Gamma_{mnpq}$ with $p \neq q$ (sector $ii$); lower panel: coupling–coupling terms of type $\Gamma_{mnpq}$, with $m < n, p < q, m \leqslant p, n \leqslant q$ (sector $iii$). Blue dots represent coupling autocorrelations, i.e. terms $\Gamma_{mnmn}$. Each colored stripe delimits all the possible combinations of the kind $mnpq$ for each pigment index $m$.

of $\Theta$, we take a pragmatic approach by focusing on its upper bound, that is set by the intrinsic excitonic timescales. In particular, we have chosen $\Theta = 1$ ps, which is comparable to the typical exciton transfer timescales found in [12] for the PE545 complex.

## 3. HSR coefficients: the white noise approximation

An overall view of the relevant Haken–Strobl couplings obtained with this method provided in figure 3, where we separately plot the elements of kind (i)–(iii) up to the permutations stated in equation (4). Here, in order to represent the elements $\Gamma_{mnpq}$ unambiguously, we have introduced an octal integer $w$ ranging from 0 to 7777, whose digits are $mnpq$. For each sector, we therefore plot the nonvanishing coefficients $\Gamma_w$ obtained from the method described in section 2. Consistently with other studies [11], we find that the relevant contribution (order 100 $\mathrm{cm}^{-1}$) in the tensor $\Gamma_w$ is given by the diagonal terms $\Gamma_{mmmm}$ in sector $i$. Notice, however, that these terms display a clear dependence on the pigment site $m$ with an approximate correlation induced by the global geometry of the complex, as also emphasized in [26]—see, for instance, the two lowest terms $\Gamma_{6666}$ and $\Gamma_{7777}$, which correspond to 'antipodal' pigments PEB 82C and PEB 82D in figure 1. Still within sector $i$, we have found no relevant contributions from site-energy cross correlations—i.e. $\Gamma_{mmnn}$ with $m \neq n$. This is consistent with a previous study by Schulten *et al* for the FMO complex [34], and reinforces the idea that in general fluctuations in the excitation energies on different pigments are not significantly correlated on the time scales of exciton transfer. Concerning sector $ii$ correlations, the maximum amplitude of $\Gamma_w$ is of order 1 $\mathrm{cm}^{-1}$ in absolute value. Moreover, we find that large couplings typically correspond to anticorrelations (i.e. negative $\Gamma_w$) between the site energy of a pigment $m$ and a coupling involving *the same* pigment $m$, i.e. for $w = mmmn$ or $w = mmnm$ with $m \neq n$. This last property was already spotlighted in [35] from the analysis of static correlation functions. A more detailed presentation of the environment couplings in sector $ii$ is provided in the supplemental material.

Here, we observe that the largest couplings that emerge in this sector are $\Gamma_{4445} = -1.8$ $\mathrm{cm}^{-1}$ and $\Gamma_{5545} = -1.4$ $\mathrm{cm}^{-1}$ (see the central panel of figure 3). These correspond to the correlations between the site energies and the coupling of the strongly-interacting central pair of pigments PEB 50/61C and PEB 50/61D—see figure 2. It is therefore not surprising that all the other couplings in sector $ii$ are significantly smaller than these two. Moreover, according to the analytical results found by Chen and Silbey [13] in the HSR model, environment couplings in sector $ii$ are expected to trigger population oscillations depending on the difference $\Gamma_{mmmn} - \Gamma_{nnmn}$. Since the relevant terms $\Gamma_{4445}$ and $\Gamma_{5545}$ have the same sign, and comparable absolute amplitude, we do not expect any relevant phenomenon related to long-lived oscillations in the HSR approximation.

Moving finally to sector $iii$, figure 3 shows that the amplitude of all $\Gamma_w$ falls below 0.1 $\mathrm{cm}^{-1}$ except for the term $\Gamma_{4545}$ which is representative of the coupling autocorrelations of the central couple of pigments. More generally, we find that the non-vanishing terms in this sector typically correspond to coupling autocorrelations, in the form $\Gamma_{mnmn}$ with $m \neq n$, (see the blue dots in figure 3). On the other hand, coupling cross correlations $\Gamma_{mnpq}$ with $m \neq n$, $p \neq q$ and $mn \neq pq$ provide a marginal contribution to sector $iii$, typically of the order of $10^{-3}$ $\mathrm{cm}^{-1}$.

A complementary view on the extracted coefficients $\Gamma_{mnpq}$ can be obtained from the information on the associated characteristic spectral widths $\omega_{mnpq}$. In figure 4 we show for each sector the hystogram of the parameters $\omega_{mnpq}$ that correspond to nonvanishing HSR coefficients of figure 3. While site energy autocorrelations (sector $i$) display a fast decay (of order 0.1 ps), correlations in sectors $ii$ and $iii$ decay with timescales that are comparable with the typical exciton timescales [12]. More precisely, we find the following ordering with respect to average decreasing $\omega_c$: site-energy autocorrelations, site-energy-coupling correlations, coupling cross correlations, coupling autocorrelations. This analysis proves that coupling–coupling autocorrelations lie at the limits of validity of the white-noise approximation intrinsic to the HSR approach. In this sense, exciton transport in proteins possibly requires

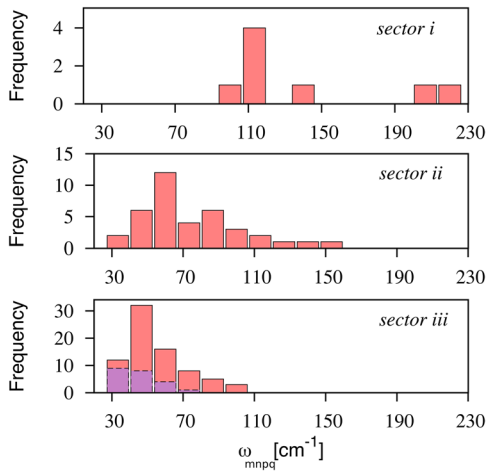


**Figure 4.** Histograms of the spectral widths $\omega_{mnpq}$ extracted by fitting a Lorentzian line shape to the cosine Fourier transforms of the correlation functions $C_{mnpq}(\omega)$ in the range $[0, 500]\,\mathrm{cm}^{-1}$. The three panels show the distribution of $\omega_{mnpq}$ in each correlation sector. For sector *iii* the purple bars refer to coupling–coupling autocorrelations, i.e. to $\omega_{mnmn}$ with $m \neq n$. Histograms are computed for $\omega_{mnpq} \geqslant 2\pi/\Theta \simeq 33\,\mathrm{cm}^{-1}$.

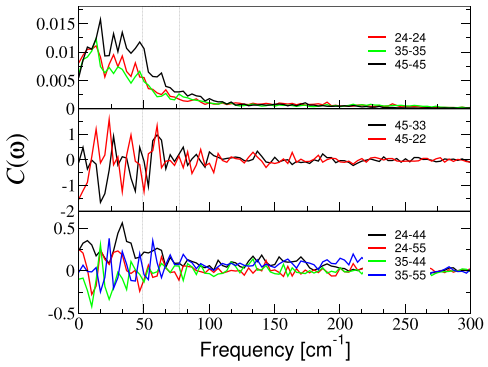


**Figure 5.** Cosine Fourier transform of selected auto and cross correlation functions. For example, the black and red lines in the middle panel refer to the cross correlations between the fluctuations of the PEB50/61C-PEB50/61D coupling (45) and the PEB158D (3) and PEB158C (2) site energies, respectively. The numbering of pigments is as illustrated in figure 2. The vertical dashed lines delimit the frequency region where our ENM analysis identify normal modes expressing concerted motions of the sub-network of CYS residues covalently linked to the pigments through disulfide bridges (see text). The spectra in the upper panel have been normalized to unit area for the sake of clarity. The others have units of cm.

more sophisticated methods, such as used in organics semiconductors, where it is known that coupling–coupling fluctuations are dominated by low-frequency, collective vibrations of the molecular crystal [36–38]. More precisely, in the case of the PE545 protein it turns out that signatures of slow frequency components emerge in the correlations among selected coupling and/or site energy fluctuations. A few typical examples illustrating this behaviour are reported in figure 5. Fluctuations with frequencies of the order of a few tens of $\mathrm{cm}^{-1}$ are likely to flag low-frequency, collective normal modes (NM) of the protein matrix, which could potentially spotlight important, fold-rooted motions expressed by the protein scaffold with the aim of selectively promoting transport by helping break localization of exciton wave-functions induced by disorder in the site energies [4, 6]. In section 4 we shall dig further into this hypothesis, with the aim of uncovering whether the PE545 protein structure is indeed able to express specific, potentially functional, transport-enhancing normal modes in the highlighted frequency range. In the next section, we stick to the white-noise approximation, and turn to investigate the effect of the QM/MM-based correlations on exciton transport.

### 3.1. Exciton transfer efficiency

The exciton transfer process can be quantified by means of two simple indicators, namely the transfer efficiency $\eta$ and the average transfer time $\bar{t}$ [4]. These quantities can be computed simply in terms of time evolution of the one-exciton density matrix,

$$\eta = 2\sum_m \kappa_m \int_0^\infty \mathrm{d}t \langle m|\rho(t)|m\rangle \qquad (10)$$

$$\bar{t} = \frac{2}{\eta}\sum_m \kappa_m \int_0^\infty \mathrm{d}t\, t\, \langle m|\rho(t)|m\rangle. \qquad (11)$$

The presence of a finite recombination rate $\alpha_m$ in equation (5) introduces a non-specific channel for exciton losses, that reduces the energy flux towards the specific trapping site. Therefore, the efficiency parameter $\eta \in [0, 1]$ quantifies the probability that an exciton is successfully driven to the trap before it recombines. A typical value of $\alpha_m$ is estimated to be independent of $m$ and of order $1\,\mathrm{ns}^{-1}$ [4]. On the other hand, we assume the presence of a single trapping site located on the lowest-energy pigment ($m = 1$) ($DBV_{19B}$) [12] with trapping rate of $1\,\mathrm{ps}^{-1}$. In order to explore the role of environment fluctuations in equation (6), we introduce a linear dependence of $\Gamma_w$ on the system temperature $T$, namely $\Gamma_w(T) = (T/T_r)\Gamma_r$ where $T_r = 300$ K denotes room temperature and $\Gamma_r$ is the coupling tensor at $T = T_r$ computed from QM/MM simulations as discussed in section 3.

In figure 6 we show the parameters $\eta$ and $\bar{t}$ as a function of temperature for an exciton initially localized on pigment PEB50/61D (site $m = 5$), i.e. one of the bilins forming the central pair of strongly interacting pigments (see figure 2). Similarly to previous studies on the FMO complex [4], we find that at room temperature $T = T_r$, the PE545 complex has almost reached the condition of maximum efficiency and minimum transfer time. Moreover, this quasi-optimum condition is by all practical means rather insensitive to temperature (note the logarithmic scale on the $x$-axis) in a range of temperatures where it can be safely asserted that the protein is in its folded, fully functional structure. It is worthwhile to observe that

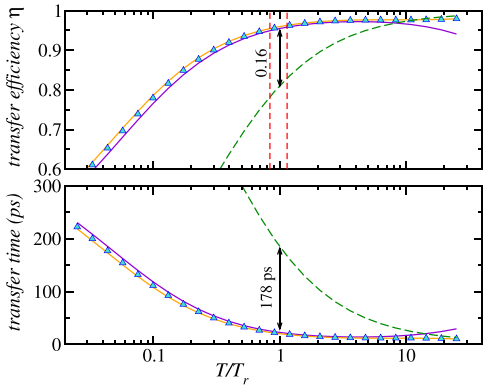


**Figure 6.** Exciton transfer efficiency (top) and average transfer time (bottom) as a function of temperature for the exciton Hamiltonian $H_0$. The purple curve refers to the evolution where only site energy fluctuations are allowed (pure dephasing noise). The orange curve accounts for the dynamics in equation (6) with the full tensor $\Gamma_w$ shown in figure 3, while cyan triangles are obtained considering only site energy autocorrelations and coupling autocorrelations. The green dashed line shows the result obtained from a purely incoherent population transfer—see equation (12). The arrows identify the differences between the quantum and classical (purely incoherent) models at room temperature, while the vertical dashed lines in the top panel identify the typical stability region of proteins, $(240 \pm 17 < T < 343 \pm 14)$ K [39]. Simulations refer to dissipation rates $\alpha_m = \alpha = 1\,\mathrm{ns}^{-1}$ and $\kappa_m = \kappa\,\delta_{1,m}$ with $\kappa = 1\,\mathrm{ps}^{-1}$.

this temperature range is rather narrow, typically $\pm 50$ K around room temperature. It is evident from figure 6 that the efficiency and average transfer times are rather constant in this temperature range (see vertical dashed lines in the top panel). It should be borne in mind that, strictly speaking, it is meaningless to consider exciton transport in light-harvesting systems outside this temperature range.

In order to gain a deeper insight into the overall transport phenomenon, we have repeated the same numerical experiment by selectively 'silencing' parts of the dynamical contributions appearing in equation (6). A first important result is that, for the wide range of temperatures here considered (biologically relevant and irrelevant), negligible variations are observed upon neglecting all the possible cross-correlations in $\Gamma_w$ (see cyan triangles in figure 6). This suggests that cross correlations in sectors *ii* and *iii* do not play a relevant role for the transport properties of the bilin complex. A complete definition of HSR coupling parameters in the limit of vanishing cross correlations is provided in the supplemental material. Further insight can be gathered from a further reduction of $\Gamma_w$ to a diagonal tensor with non-vanishing elements of kind $\Gamma_{mmmm}$, i.e. the coefficients shown in the upper panel of figure 3. The above approximations lead to the usual description of environmental effects in terms of *pure dephasing* noise, where optimal transport was shown to emerge [4] for a *finite* dephasing rate. It is clear from figure 6 that the characteristic high-temperature efficiency drop (associated in [4] with the quantum Zeno effect [27]) is no longer present when generalized correlations beyond pure dephasing are considered. This result is a direct consequence of the presence of small but non-vanishing coupling fluctuations, i.e. of terms $\Gamma_{mmnn}$ with $(m \neq n)$, which promote a population transfer between sites $m$ and $n$ [13–16]. A similar effect was recently observed in [28, 40] within the framework of an explicit nonlinear quantum-classical hybrid model. As a general observation, we emphasize that the Zeno-like decrease in efficiency associated with pure dephasing falls in a temperature range where the protein matrix would be in a wildly denatured state, which means that such regime is by all means not biologically relevant, and could not possibly have been accessed by evolution. We observe that this conclusion would hold *a fortiori* were the mapping between temperature and strength of correlations nonlinear, i.e. $\Gamma_w(T) = (T/T_r)^\nu \Gamma_r$ with $\nu > 1$.

The high-temperature regime can be captured by a simple master equation for purely incoherent population transfer (a classical random walk) in the form

$$\frac{\mathrm{d}\rho_{nn}}{\mathrm{d}t} = \sum_{m \neq n} \Gamma_{nmnm}\rho_{mm} - \rho_{nn} \sum_{m \neq n} \Gamma_{nmnm} \quad , \qquad (12)$$

where only coupling autocorrelations are considered (see green dashed line in figure 6). Equation (12) is essentially a Fokker–Planck equation for the classical occupation probability $\rho_{nn}$ on pigment $n$. As shown in figure 6, the purely classical description approaches the generalized HSR dynamics in the region $T \gtrsim 10\,T_r$. It is worth noting that the purely diffusive description underestimates the transfer efficiency by about 17% (and correspondingly overestimates the average transfer time of a larger factor of about eight) in the biologically relevant temperature region (see arrows in figure 6), suggesting that some degree of coherence is indeed important in achieving optimal transport.

From the previous analyses, it is clear that a certain amount of noise is required to break disorder-induced localization of the exciton caused by the heterogeneity of local site energies. An interesting question to ask concerns the role of the specific *realization* of such noise, in terms of the correspondence between the elements of the tensor $\Gamma_{mnpq}$ and specific pairs of pigments in the structure. One simple way to address this question is to investigate the effect on transport of randomly reshuffling the tensor elements. For this purpose, one can restrict to site-energy and coupling–coupling autocorrelations (it is clear from figure 6 that this will not induce appreciable differences on the results). In terms of the associated tight-binding network (see figure 2), this amounts to randomly rewiring the nodes. Figure 7 shows efficiency curves computed for a large number of independent random rewiring realizations. Each of this corresponds to a different random reshuffling of the pairs $(J_{nm}, \Gamma_{nmnm})$, with $n \neq m$, i.e. pigment couplings and associated pigment–pigment noise. It is clear that in the physically relevant region close to

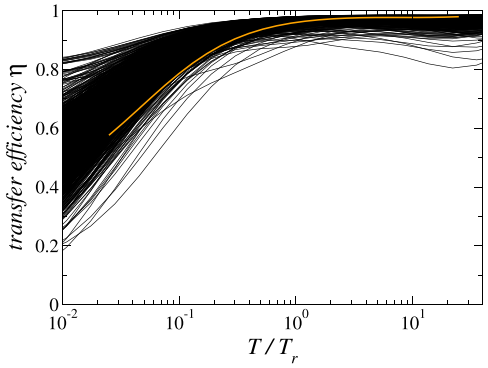


**Figure 7.** Exciton transfer efficiency as a function of temperature for different modified Hamiltonians obtained by randomly reshuffling the off-diagonal elements $J_{nm}$ of $H_0$ (see equation (1)) and the corresponding QM/MM fluctuations (corresponding to coupling–coupling autocorrelations). Simulations refer to 1000 independent reshufflings. Other parameters were set as in figure 6. The orange line denotes the results shown in figure 6 obtained with the full tensor $\Gamma_w$ shown in figure 3.

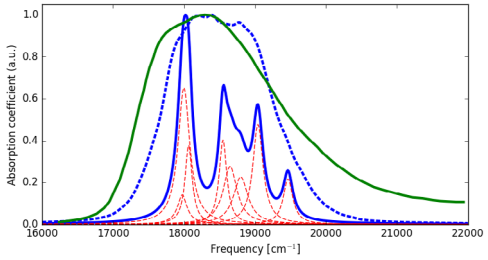


**Figure 8.** Linear absorption spectra of the PE545 complex. The green line is a plot of the experimental data from [12]. The thick blue line is the theoretical spectrum computed through equation (A.9), with the red dashed lines depicting the individual (weighted) Lorentzian contributions marking the excitonic frequencies. The blue dashed line is the theoretical spectrum including inhomogeneous broadening due to static disorder, i.e. Gaussian noise on the excitonic levels with $\sigma = 600\ \mathrm{cm}^{-1}$ [43]. This is accomplished by averaging many ($10^3$ here) spectra (14) corresponding to random Hamiltonians $\langle n|H_0^s|m\rangle = (\epsilon_{nm} + \Delta\epsilon)\delta_{nm} + (J_{nm} + \Delta J)(1 - \delta_{nm})$, with $\Delta\epsilon$, $\Delta J$ random Gaussian deviates with zero mean and standard deviation $\sigma_\epsilon = 330\ \mathrm{cm}^{-1}$ and $\sigma_J = 1.1\ \mathrm{cm}^{-1}$ respectively. The ratio $\sigma_J/\sigma_\epsilon \approx 0.0033$ has been chosen to match the results of the QM/MM simulations reported in [12]. The average transition dipole moments used in this calculation are also from [12].

$\Gamma_r$, deviations from the efficiency corresponding to the *true* set of physical parameters are negligible. Analogous results were obtained when considering random reshufflings of site energies and associated noise terms, i.e. the pairs $(J_{mm}, \Gamma_{mmmm})$, or combinations of both strategies. Moreover, deviations of the same order of magnitude were obtained for the corresponding average transfer times (results not shown).

Overall, this analysis seems to suggest that high transport efficiency in a tight-binding model with site disorder can be achieved robustly through noise, rather insensitively of the specific connectivity pattern of the tight-binding network. At the same time, one should be warned that efficiency is a rather *global* indicator. Therefore, some caution is required in interpreting this result as a thorough dismissal of tight and specific connections between the physical and geometrical structures underlying noise correlations and the propagation of quantum excitations coupled to the vibrating, noise-producing scaffold. Moreover, explicitly disregarding certain slow frequency components in the spectral densities, in accordance with the white noise prescription, could prove a crucial limitation in the quest for quantitative links between protein vibrations and exciton transport. All in all, although certain general properties of exciton transport can be successfully understood within simplified treatments like the HSR model, one should probably couple these with more refined quantum-classical hybrid methods, which have recently become feasible even for very large systems [41], and where structure-encoded spatiotemporal correlations provide an *explicit* description of all protein vibrations.

### 3.2. Linear absorption spectra

The linear absorption spectrum (LAS) is given by the Fourier transform of the (transition) dipole autocorrelation function [25, 30, 42], that is,

$$\alpha(\omega) \propto \omega\, \mathrm{Re} \int_0^\infty \mathrm{e}^{\mathrm{i}\omega t} \langle \boldsymbol{\mu}(t) \cdot \boldsymbol{\mu}(0) \rangle \, \mathrm{d}t. \qquad (13)$$

The LAS is an easily measurable quantity, and is often employed in the literature in the field of natural and artificial light-harvesting systems as a reference experimental observable against which to test various theoretical approaches. It is therefore interesting to elaborate on this point in the context of our treatment. In principle, in the reasonable hypothesis that the electronic ground state (i.e. zero excitons) is not coupled to the single excitation manifold or the bath, the dipole autocorrelation function can be computed from the knowledge of the system Liouville time-operator [30, 40]. In practice, it does not seem immediately straightforward to perform this calculation including the entire correlation tensor $\Gamma_{abcd}$. This problem will be tackled in forthcoming publications. For the moment, we will only consider noise associated with site energy self-correlations, i.e. terms of the kind $\Gamma_{aaaa}$ only, which extends the known result obtained for master equations with constant pure-dephasing noise, i.e. with $\Gamma_{aaaa} = \gamma_0\ \forall\, a$ (see e.g. [40]). The details of this calculations are reported in appendix A. The result is still a weighted sum of Lorentzian lineshapes:

$$\alpha(\omega) \propto \omega \sum_{n,m,k} \frac{\gamma_m \boldsymbol{\mu}_n \cdot \boldsymbol{\mu}_m \langle n|k\rangle\langle k|m\rangle}{\gamma_n^2 + (\omega - \omega_k)^2} \qquad (14)$$

where $\gamma_n = \Gamma_{nnnn}$, $\omega_k$ and $|k\rangle$ are the exciton eigenvalues and eigenvectors respectively, and $\boldsymbol{\mu}_n$ denotes the average transition dipole vector at site $n$. The linear absorption coefficient (14) plotted in figure 8 (dashed blue line) shows that homogeneous

broadening, i.e. the effect of thermal noise, preserves distinct features of the individual exciton lines. In fact, it is only by adding the effect of static disorder (inhomogeneous broadening) that one recovers a spectrum that looks like the experimental one. This is the effect that arises as the same pigment sits in slightly different local environments in different PE545 proteins. The deviations observed between our simple theory and experiments is likely due to the fact that here we are not accounting for the additional homogeneous broadening given by the inverse lifetime of the exciton states (i.e. related to transitions between different exciton states), typically ranging in the 10–100 $\mathrm{cm}^{-1}$ interval [42], and slow fluctuations cannot be explicitly incorporated in HSR theory, which by construction assumes that noise is only coming from fast phonon modes. In fact, a better agreement can be found by including the latter factors, such as in the modified Redfield theory approach described in [25]. However, one should observe that often in such approaches the phonon modes included in the spectral density are treated as free parameters, e.g. adjusted on other experimental data sets, such as fluorescence spectra [25].

It is worth noting that a typical value for inhomogeneous broadening, i.e a standard deviation of the order of 600 $\mathrm{cm}^{-1}$ [43], is approximately two to three times larger than the typical dephasing rates used in this and other studies, fixed by the typical decorrelation time of site energy fluctuations, which is of the order of $10^2$ fs. We conclude that, even if the overall agreement between our averaged theoretical spectrum and the experimental data is not perfect, it appears that, as it happens for the transfer efficiency, the LAS makes it hard to discriminate between theoretical descriptions of the exciton–phonon coupling. We remark that the fact that LAS in these systems are strongly inhomogeneously broadened is a well established fact [25, 42].

In order to investigate the direct link between vibrational dynamics of the scaffold and exciton dynamics, it is interesting to couple the results of QM/MM simulations with simple but powerful theoretical schemes used to explore the structure-dynamics relation in the protein scaffold that envelops the pigment network. In the next section, based on the spectral features emerging from the correlations computed through QM/MM simulations, we develop a general method to dig for possible exciton-coupled vibrational patterns of the protein matrix.

## 4. HSR coefficients: an elastic-network analysis reveals specific low-frequency normal modes

In this section, we consider the question of whether the slow-frequency components emerging in certain QM/MM-based spectral densities (see again figure 5) flag specific *collective vibrations*, whose pattern is encoded in the protein scaffold and that would selectively couple to exciton transport at the limits of validity of the HSR approach.

The elastic-network model (ENM) denotes a class of powerful and rather inexpensive tools that are well suited to the investigation of collective fluctuations of proteins [44–48]. In the residue coarse-grained (CG) version, also known as the anisotropic network model (ANM) [44], the protein is described as a network of as many fictive beads as there are amino acids. In the simplest case, each bead possesses the same mass, equal to the average amino acid mass (about 110 a.m.u.), and occupies at rest the position of the corresponding $\alpha$ Carbon along the backbone chain of the protein as determined from an experimentally solved structure, i.e. x-ray or NMR. The beads interact through identical Hooke springs with other beads in the structure located within a specified cutoff distance $R_c$. According to this prescription, the total potential energy of such elastic network model reads [7]

$$U = \frac{1}{2} k_2 \sum_{i>j=1}^{N} c_{ij} (r_{ij} - R_{ij})^2 \qquad (15)$$

where $N$ is the number of residues; $R_{ij}$ and $r_{ij}$, the equilibrium and instantaneous distances, respectively, between residues $i$ and $j$; and $k_2$, the common spring stiffness. The matrix $c_{ij}$ specifies the connectivity of the network: $c_{ij} = \{1 \text{ for } R_{ij} \leqslant R_c | 0 \text{ otherwise}\}$. Consensus choices for the two parameters of such a model are $k_2 = 5$ kcal $\mathrm{\AA}^{-2}$ and $R_c = 10$ $\mathrm{\AA}$ [50]. The normal modes can be easily computed as the eigenvectors of the Hessian matrix of the potential energy function (15) [51]. With this choice of the parameters, the coarse-grained NM spectrum of PE545 (PDB id. `1XG0`) spans the frequency interval $[3.9 - 93.5]\,\mathrm{cm}^{-1}$.

All chromophores in the PE5454 complex are covalently linked through disulfide bridges to specific cysteine residues (CYS) [23]. The central pigments PEB50/61C and PEB50/61D form two disulfide bridges each, while all the other bilins are covalently linked to one cysteine residue each. Overall, these residues form an extended subnetwork of anchor points, whose concerted motions are likely to influence the coupling and site energy fluctuations of the attached pigments. It is instructive to investigate how the average and the standard deviation of the QM/MM coupling time series depend upon the distance between the respective covalently linked CYS pairs. The data reported in figure 9 suggest that on average both indicators referring to a given pair of pigments decrease with the distance between the associated CYS anchor points (dashed lines). Interestingly, pairs associated with slow frequency components in the corresponding spectral densities (see figure 5) stand out from the common average trend as outliers. More precisely, fluctuations (gauged here by the standard deviations) of the 53 and 42 pairs are seen to be anomalously large

[7] See [49] for a thorough discussion of alternative schemes.

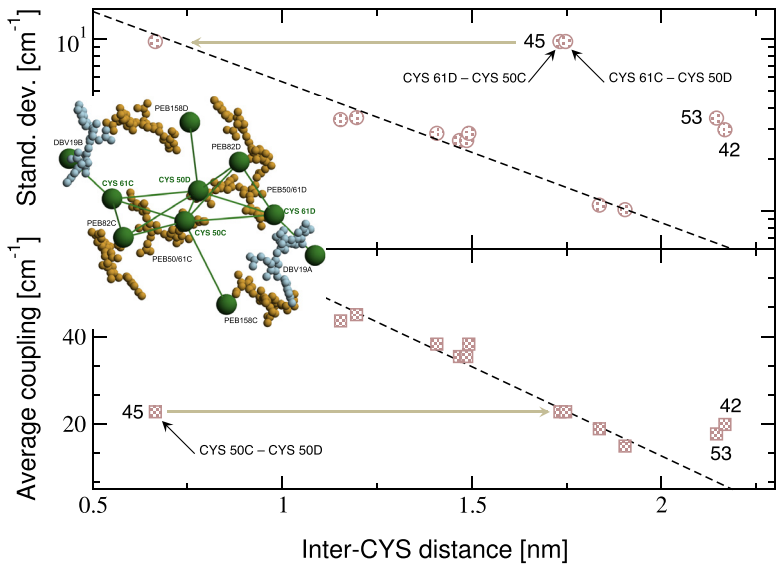


**Figure 9.** Average absolute value (bottom) and standard deviation (top) of the QM/MM coupling time series [12] versus distance between the covalently attached cysteine residues (computed from the PE545 PDB structure, PDB id. 1XG0). The dashed lines are plots of the apparent *typical* trends, namely the exponential decay $\sigma(d) = \sigma_0 \exp(-d/d_\sigma)$, with $\sigma_0 = 37.21\,\mathrm{cm}^{-1}, d_\sigma = 5.3$ Å (top) and $\langle J(d)\rangle = J_0(1 - d/d_c)$, with $J_0 = 94.4\,\mathrm{cm}^{-1}, d_c = 23.1$ Å. The inset diagram shows the sub-network of covalently attached cysteine residues and the links flag the shortest 15 CYS-CYS inter-distances, from the closest pair, namely CYS 50C and CYS 50 D (6.65 Å), to the pair CYS158C-CYS50C (21.67 Å). The couplings that appear to be outliers with anomalously large fluctuations and off-trend average couplings are explicitly highlighted (the numbering is the same as that used in figure 2). 53: CYS 50D-CYS 158 D, 42: CYS 50C-CYS 158D.

as compared to the average trend at the same CYS–CYS distances. This is all the more remarkable in that it concerns pairs located at large distances. Another interesting observation is that the average coupling of the central PEB pair (45) appears to be on the common trend only when associated with pairs of opposite cysteines (61C–50D and 61D–50C, see again the cartoon and the arrow in the bottom panel of figure 9). However, this is no longer true for the corresponding fluctuation, which appears to be of the correct order of magnitude only when associated with the two central cysteines (50C–50D, top horizontal arrow). Overall, this suggests that the fluctuations in the 54 coupling are controlled by the relative motions of the CYS50C–CYS50D pair. In turn, this points to the interaction between the associated terminal pyrrole rings (nearly parallel and about 5 Å away from each other) as the main structural unit controlling the fluctuations of the 45 coupling strength.

The above observations strongly suggest that there exist a subset of normal modes in the 30–80 $\mathrm{cm}^{-1}$ range whose displacement field (pattern) represents specific concerted motions of the cystein subnetwork. Such modes, showing up in the spectral density referring to specific coupling–coupling and coupling-site energy (cross) correlations, are good candidates in the quest for fold-encoded, transport-enhancing vibrations. In order to identify these modes, we have proceeded as follows. First, we have ranked normal modes in descending order with respect to their involvement fraction on the CYS subnetwork. Let us denote the latter as $\mathcal{S}_{\mathrm{cys}}$ and let $\vec{\xi}_i^k$ denote the displacement of particle (residue) $i$ in the mode $k$. NMs patterns are normalized, i.e. $\sum_{i=1}^{3N-6} |\vec{\xi}_i^k|^2 = 1 \;\forall\, k$, so that the quantity

$$f_k = \sum_{i \in \mathcal{S}_{\mathrm{cys}}} |\vec{\xi}_i^k|^2 \leqslant 1 \tag{16}$$

gauges the relative weight of the covalently linked cysteines in the overall displacement field of the $k$th NM. If only those residues were vibrating in a given mode $m$, one would have $f_m = 1$.

It would be tempting to rank all normal modes in descending order with respect to the associated $f_k$ values, and select the top-scoring ones. However, a moment's thought is enough to realize that one also needs to gauge the *statistical significance* of a given $f_k$ score. This should be done by considering for each mode the null hypothesis that a totally random subset of as many residues would give the same score. Thus, for each NM we have computed a $p$-value by performing a large number $N_R = 10^4$ of random reshufflings of the NM pattern and computing the corresponding value of the involvement score $f_k^R(i), i = 1, 2, \ldots, N_R$. The statistical significance of the measured involvement for a given NM can then be estimated by the fraction of random scores exceeding the measured one. Specifically,

$$p_f = \frac{1}{N_R} \sum_{i=1}^{N_R} \Theta\left(f_k^R(i) - f_k\right) \tag{17}$$

where $\Theta(x)$ is the Heaviside function. The quantity $1 - p_f$ gauges the rejection probability of the null hypothesis. If we restrict to confidence levels greater than 95%, this analysis singles out 78 NMs with

**Table 1.** Values of $\mu_{ij}$ for different pairs in the CYS-CYS subnetwork for the eight normal modes with $p_f, p_\mu < 0.05$ The figure $\overline{\mu}$ is the average value over the considered 15 pairs (see text). The last column reports the $\mu$-confidence level (c.l.), i.e. $1 - p_\mu$. Normal modes are numbered starting from the highest frequency one.

| NM | $\omega$ [cm$^{-1}$] | $\overline{\mu}$ | 50C–50D | 61D–50C | 50D–61C | 158D–50D | 158C–50C | c.l. |
|---|---|---|---|---|---|---|---|---|
| 144 | 77.49 | 0.639 | −0.915 | −0.750 | 0.888 | 0.251 | 0.386 | 0.974 |
| 245 | 72.45 | 0.691 | 0.866 | 1.000 | −0.659 | 0.215 | −0.974 | 0.995 |
| 432 | 65.74 | 0.636 | −0.706 | 0.475 | −0.770 | −0.380 | −0.585 | 0.972 |
| 501 | 63.37 | 0.639 | 0.900 | −0.901 | −0.478 | 0.904 | 0.750 | 0.971 |
| 531 | 62.39 | 0.635 | 0.731 | 0.994 | −0.853 | −0.605 | 0.146 | 0.963 |
| 546 | 61.87 | 0.764 | −0.991 | 0.317 | 0.634 | −0.980 | 0.850 | 1.000 |
| 556 | 61.50 | 0.650 | 0.402 | −0.814 | 0.965 | −0.505 | 0.652 | 0.976 |
| 940 | 48.57 | 0.623 | 0.941 | 0.104 | 0.904 | 0.927 | −0.669 | 0.953 |

frequencies lying between $\omega_1 = 31.98$ cm$^{-1}$ and $\omega_2 = 77.49$ cm$^{-1}$, i.e. 6.9% of the NMs in the same frequency range and 5.3% of the total number of NMs. We term this ensemble $\mathcal{M}_{95}$. Interestingly, this is precisely the same frequency range where low-frequency structures appear in specific spectral-densities (see again figure 5). It is possible to refine further the choice of possible interesting NMs by isolating vibrations whose vibrational patterns are mostly directed along the directions joining pairs of cysteines in the covalent subnetwork. We isolated the closest 15 pairs, which correspond to two links in the connectivity graph ($R_c = 10$ Å, inter-distances shorter than 21.67 Å, see cartoon in figure 9). For each NM, we computed the projection

$$\mu_{ij}^k = \frac{\vec{\xi}_i^k - \vec{\xi}_j^k}{\left|\left|\vec{\xi}_i^k - \vec{\xi}_j^k\right|\right|} \cdot \hat{R}_{ij} \qquad (18)$$

where $\hat{R}_{ij}$ denotes the unit vector joining cysteine $i$ to cysteine $j$ in the equilibrium structure. Again, one needs to evaluate the rejection probability of the null hypothesis, stipulating that a value of $\mu$ equal or higher than a measured one can be obtained by selecting 15 random pairs of residues in the entire structure. We then considered the NMs in the previously identified subset $\mathcal{M}_{95}$ and computed the indicators $\mu_{ij}^k$ and their associated $p$-values, defined as

$$p_\mu = \frac{1}{N_R} \sum_{i=1}^{N_R} \Theta\left(\overline{\mu}^R(i) - \overline{\mu}^k\right) \qquad (19)$$

where $\overline{\mu}$ refers to the average of the projections (18) computed over the 15 closest cysteine pairs ($\overline{\mu}^k$) and over as many randomly selected pairs ($\overline{\mu}^R$) for a given normal mode $k$ in the subset $\mathcal{M}_{95}$.

Remarkably, 10% of these modes (eight NMs out of 78) showed a confidence level $1 - p_\mu$ greater than 95%. A summary of this analysis is reported in table 1. Such modes have frequencies in a somewhat narrower range than the previous 78 ones, lying in the range [48.57,77.49] cm$^{-1}$ (see vertical lines in figure 5). The average projection on the first 15 CYS-CYS inter-distances over the whole subset is 0.66, suggesting that these NMs are indeed concerted motions of the CYS-CYS subnetwork, whose vibrational patterns can be imagined to a great extent as acting along the links of the associated connectivity subgraph (see green sticks in the cartoon in figure 9). Remarkably, the average projection $\mu_{ij}$ on the 50C–50D direction (corresponding to the largest QM/MM coupling fluctuation) is 0.81, larger than the average projection computed for all the 15 pairs. This strongly confirms our previous inference about the crucial role of these two cysteines in mediating the protein-encoded fluctuations that couple to exciton transport.

## 5. Conclusions and perspectives

In this paper, we have provided a realistic parametrization of the Haken–Strobl model (6) for the PE545 bilin complex from QM/MM simulations. The aim of our analysis was to dig for the different auto- and cross-correlations relating to pigment site energies and pigment–pigment couplings, and investigate their role on exciton mobility. We have used this approach to characterize exciton transport by means of simple global observables, namely the transport efficiency and the average transfer time. As a result, we have found that at room temperature the system is very close to the optimal transport regime with a predominant contribution from site-energy fluctuations. Moreover, in the optimal regime the transport efficiency is rather insensitive to random reshuffling of the elements of the Hamiltonian and the associated noise tensor. This suggests that noise-induced depinning of quantum excitations in disordered environments is a rather general feature of open quantum systems.

The high temperature regime revealed that the small residual coupling fluctuations in the dynamics suppress the quantum Zeno regime at temperatures $T \gtrsim 5\, T_r$, where the dynamics is essentially that of a classical random walk. Although this regime is not meaningful from a biological standpoint, since proteins unfold at temperatures $T \gtrsim 1.2\, T_r$, our study provides a different reading frame for noise-assisted quantum transport [4] in photosynthetic complexes. Specifically, the effect of environment fluctuations at room temperature is to provide access to *the same*

efficiency level that would pertain to an inaccessible regime of classical diffusion at extremely high temperatures. To put it in more evocative terms, one might argue that evolution has taken advantage of the laws of quantum mechanics to lower the effective temperature corresponding to the highest efficiency (the classical regime) to the region of working temperatures of proteins in a living organism.

We have shown that QM/MM data spotlight clear slow frequency components in the [30–80] $cm^{-1}$ range in the spectral densities associated with specific coupling–coupling and coupling-site energy fluctuations. Typically, these involve the central PEB50/61D/C pigments. These lie at the threshold of validity of the white noise approximation inherent in HSR-type approaches, relaxing in time as fast as or more slowly than the timescale associated with exciton transfer.

While there seems to be no obvious way to include slow, collective modes in HSR-type descriptions of exciton transport, in the last section of the paper we lay out a possible strategy to tackle this problem through the elastic-network model formalism. Our analysis clearly identifies a set of specific collective normal modes that preferentially couple the subnetwork of ten cysteine residues covalently linked to bilins. Such modes, selected through an original double statistical-significance analysis, have the combined properties of (i) maximum concerted involvement on the CYS subnetwork and (ii) maximum displacement *alignment* with the ensemble of the closest inter-distance vectors between cysteine pairs. These modes, with frequency lying in the [50–80] $cm^{-1}$ range, might be important fold-encoded *noise* sources for enhancing exciton transport optimally within the pigment-hosting protein matrix. More generally, this analysis could be repeated in other light-harvesting structures to identify possible vibrational patterns directly connected to the embedded pigment sub-network.

We stress that the slowest correlations found in the QM/MM fluctuation time series cannot be included in the tensor $\Gamma_{nmnm}$, as the HSR model is bound to the hypothesis of white noise (only noise from phonons faster than exciton transfer). In this sense, the conclusions of our NM analysis cannot be straightforwardly applied to the transfer efficiency analysis within the HSR model—in particular, the fact that the efficiency at high enough temperatures seems to be rather insensitive to the specific wiring of the network of pigment couplings and associated fluctuations. At low temperature, the wiring is important. If a large coupling and its associated fluctuations are assigned to the link between the starting pigment and the trap, or to a link in the shortest path between them (i.e. the minimum number of intermediate connected nodes), the efficiency will already be large at low temperature, by virtue of the large coupling. However, what our results prove is that at high enough temperature, where the non-Hermitian part of the quantum master equation becomes important, the local energy pathways of the exciton network are deeply modified (rewired), while the global transport efficiency is weakly perturbed. The fact that, on average, such random rewirings do not destroy the efficiency pattern computed for the true structure (figure 7) is mainly due to the self-averaging character of the efficiency measure within the HSR model. In fact, one might argue that rewiring within a different model able to consistently include slow components beyond the white noise approximation could have a more pronounced effect on the efficiency. To summarize, our NM analysis should be regarded as providing some insight into which slow normal modes are indeed concerted vibrations of the pigment sub-network in a given light-harvesting structure containing a sub-network of pigments. Moreover, the white-noise approximation makes a global observable such as the efficiency largely insensitive to rewiring provided the noise level is high enough.

The logical step beyond microscopically parameterized HSR approaches to investigate the above hypothesis is to turn to coarse-grained quantum-classical hybrid descriptions, often also called mixed quantum classical approaches (QCA) [52]. In QCAs, the force acting on classical degrees of freedom is computed by considering an effective potential energy given by the quantum mechanical expectation value of the system-reservoir coupling according to the instantaneous values of the classical coordinates and the wave function of the quantum degrees of freedom (DOFs). While the presence of the classical DOFs results in an additional potential for the dynamics of the quantum system, the classical reservoir feels the quantum mechanically averaged force of the relevant quantum system. This method is often referred to as the Ehrenfest method [52], and falls within the class of mean-field approaches. Interestingly, a recent QCA based on the nonlinear network model [50] has shown that specific fold-rooted vibrational modes have the potential to spotlight alternative excitation energy transfer routes in the Fenna–Matthews–Olson (FMO) complex through their influence on pigment properties [53]. Overall, also in view of the results of the previous section, elastic/nonlinear-network model-based QCAs can be regarded as optimal tools to investigate the role of specific fold-encoded vibrational modes in exciton transport in light-harvesting complexes.

## Acknowledgments

SP, SI, YO and FP thank financial support from the EU FP7 project PAPETS (GA 323901). SP and YO thank the support from the JTF project NQuN (ID 60478) and from Fundação para a Ciência e a Tecnologia (Portugal), namely through programmes PTDC/POPH/POCH and projects UID/EEA/50008/2013, IT/QuNet, ProQuNet, partially funded by EU FEDER, as well as project CRUP/CPU CQVibes TC16/14. Furthermore SP acknowledges the support from the DP-PMI and FCT (Portugal) through scholarship PD/BD/52549/2014.

## Appendix

In this appendix we compute the analytic expression for the linear absorption coefficient in the HSR model. For the sake of the argument, we restrict ourselves in this paper to the case of site energy fluctuations only. The following treatment extends the treatment of Moix *et al* [40] to the case of site-dependent dephasing rates, $\gamma_n \equiv \Gamma_{nnnn}$. Let us introduce the total average transition dipole moment operator, defined as

$$\hat{\boldsymbol{\mu}} \equiv \sum_n \hat{\boldsymbol{\mu}}_n = \sum_n \boldsymbol{\mu}_n \left(|n\rangle\langle 0| + |0\rangle\langle n|\right) \tag{A.1}$$

where $|0\rangle$ is the ground state (no exciton), $|n\rangle$ are the local site basis vectors, and $\boldsymbol{\mu}_n = \sqrt{\bar{\mu}_x^2 + \bar{\mu}_y^2 + \bar{\mu}_z^2}$ are the MD-averaged transition dipole moments computed via QM/MM simulations [12]. The linear absorption coefficient is obtained by Fourier transforming the total dipole autocorrelation function,

$$\langle \boldsymbol{\mu}(t)\cdot\boldsymbol{\mu}(0)\rangle = \sum_{n,m}\langle \hat{\boldsymbol{\mu}}_n(t)\cdot\hat{\boldsymbol{\mu}}_m(0)\rangle = \mathrm{Tr}\left[\hat{\boldsymbol{\mu}}_n(t)\cdot\hat{\boldsymbol{\mu}}_m(0)\hat{\rho}_0\right] \tag{A.2}$$

where $\hat{\rho}_0 = |0\rangle\langle 0|$ is the ground-state density matrix. Correlation functions can be evaluated by expressing them in terms of time-evolution operators. One has

$$\begin{aligned}\mathrm{Tr}\left[\hat{\boldsymbol{\mu}}_n(t)\cdot\hat{\boldsymbol{\mu}}_m(0)\hat{\rho}_0\right] &= \mathrm{Tr}\left[U^\dagger\hat{\boldsymbol{\mu}}_n U\cdot\hat{\boldsymbol{\mu}}_m\hat{\rho}_0\right]\\ &= \mathrm{Tr}\left[\hat{\boldsymbol{\mu}}_n\cdot \mathrm{e}^{-\mathrm{i}\mathcal{L}t}\hat{\boldsymbol{\mu}}_m\hat{\rho}_0\right]\end{aligned} \tag{A.3}$$

where $U = \exp[-\mathrm{i}\mathcal{H}t/\hbar]$ is the time evolution operator for the total system and the thermal bath and $\mathcal{L}$ is the corresponding Liouville time-operator, yielding the solution to the (stochastic) Liouville equation in the interaction picture

$$\rho(t) = \mathrm{e}^{-\mathrm{i}\mathcal{L}t}\rho(0). \tag{A.4}$$

Furthermore, in (A.3) we have used the cyclic invariance of the trace, and the fact that the ground state is not coupled to the single excitation manifold or the bath.

The time evolution of the partial density matrix $\hat{\rho}^{[n]} \overset{\text{def}}{=} \hat{\mu}_n\hat{\rho}_0$, with initial state $\hat{\rho}^{[n]}(0) = \hat{\mu}_n(0)\hat{\rho}_0$, in the simple case of noise associated with site energy auto-correlations only, is given by the Haken–Strobl reduced master equation, which can be written as follows:

$$\frac{\mathrm{d}\hat{\rho}^{[n]}}{\mathrm{d}t} = -\frac{\mathrm{i}}{\hbar}[\hat{\mathcal{H}}_0, \hat{\rho}^{[n]}] - \sum_p \gamma_p[\hat{V}_p, [\hat{V}_p, \hat{\rho}^{[n]}]] \tag{A.5}$$

with $\hat{V}_n = |n\rangle\langle n|$. Since the ground state is not coupled to the single excitation manifold or the bath, the above master equation reduces to

$$\frac{\mathrm{d}\hat{\rho}^{[n]}}{\mathrm{d}t} = -\frac{\mathrm{i}}{\hbar}\hat{\mathcal{H}}_0\hat{\rho}^{[n]} - \gamma_n\hat{\rho}^{[n]}. \tag{A.6}$$

Recalling (A.3), and introducing the eigenstates of the exciton Hamiltonian $|k\rangle$, with $\hat{H}_0|k\rangle = \hbar\omega_k|k\rangle$, one has ($\langle 0|n\rangle \equiv 0\ \forall\, n$)

$$\begin{aligned}\langle \boldsymbol{\mu}_n(t)\cdot\boldsymbol{\mu}_m(0)\rangle &= \mathrm{e}^{-\gamma_m t}\langle 0|\hat{\boldsymbol{\mu}}_n\cdot \mathrm{e}^{-\mathrm{i}\hat{H}_0 t/\hbar}\hat{\boldsymbol{\mu}}_m|0\rangle\\ &= \boldsymbol{\mu}_n\cdot\boldsymbol{\mu}_m\mathrm{e}^{-\gamma_m t}\sum_k \mathrm{e}^{-\mathrm{i}\omega_k t}\langle n|k\rangle\langle k|m\rangle.\end{aligned} \tag{A.7}$$

Hence, we finally get for the total autocorrelation function

$$\langle \boldsymbol{\mu}(t)\cdot\boldsymbol{\mu}(0)\rangle = \sum_{n,m,k}\boldsymbol{\mu}_n\cdot\boldsymbol{\mu}_m\mathrm{e}^{-(\mathrm{i}\omega_k+\gamma_m)t}\langle n|k\rangle\langle k|m\rangle. \tag{A.8}$$

Inserting (A.8) in the definition (13), one readily obtains the linear absorption coefficient as a weighted sum of Lorentzian lineshapes, that is,

$$\alpha(\omega) \propto \omega\sum_{n,m,k}\frac{\gamma_m\boldsymbol{\mu}_n\cdot\boldsymbol{\mu}_m\langle n|k\rangle\langle k|m\rangle}{\gamma_n^2 + (\omega-\omega_k)^2}. \tag{A.9}$$

## ORCID iDs

Francesco Piazza https://orcid.org/0000-0003-0205-3790

## References


[1] van Amerongen H, van Grondelle R and Valkunas L 2000 *Photosynthetic Excitons* (Singapore: World Scientific)

[2] Mohseni M, Omar Y, Engel G and Plenio M B (ed) 2014 *Quantum Effects in Biology* (Cambridge: Cambridge University Press)

[3] Adolphs J and Renger T 2006 How proteins trigger excitation energy transfer in the FMO complex of green sulfur bacteria *Biophys. J.* **91** 2778–97

[4] Rebentrost P, Mohseni M, Kassal I, Lloyd S and Aspuru-Guzik A 2009 Environment-assisted quantum transport *New J. Phys.* **11** 33003

[5] Caruso F, Chin A W, Datta A, Huelga S F and Plenio M B 2009 Highly efficient energy excitation transfer in light-harvesting complexes: the fundamental role of noise-assisted transport *J. Chem. Phys.* **131** 105106

[6] Plenio M B and Huelga S F 2008 Dephasing-assisted transport: quantum networks and biomolecules *New J. Phys.* **10** 113019

[7] Rebentrost P, Mohseni M and Aspuru-Guzik A 2009 Role of quantum coherence and environmental fluctuations in chromophoric energy transport *J. Phys. Chem.* B **113** 9942–7

[8] Fassioli F, Nazir A and Olaya-Castro A 2010 Quantum state tuning of energy transfer in a correlated environment *J. Phys. Chem. Lett.* **1** 2139–43

[9] Nalbach P, Eckel J and Thorwart M 2010 Quantum coherent biomolecular energy transfer with spatially correlated fluctuations *New J. Phys.* **12** 065043

[10] Wu J, Liu F, Shen Y, Cao J and Silbey R J 2010 Efficient energy transfer in light-harvesting systems, I: optimal temperature, reorganization energy and spatial–temporal correlations *New J. Phys.* **12** 105012

[11] Renger T, Klinger A, Steinecker F, Am Busch M S, Numata J and Müh F 2012 Normal mode analysis of the spectral density of the Fenna–Matthews–olson light-harvesting protein: how the protein dissipates the excess energy of excitons *J. Phys. Chem.* B **116** 14565–80

[12] Curutchet C, Novoderezhkin V I, Kongsted J, Auroraoz-Losa A M-L, Van Grondelle R, Scholes G D and Mennucci B 2013 Energy flow in the cryptophyte PE545 antenna is directed by bilin pigment conformation *J. Phys. Chem.* B **117** 4263–73

[13] Chen X and Silbey R J 2010 Effect of correlation of local fluctuations on exciton coherence *J. Chem. Phys.* **132** 204503

[14] Vlaming S M and Silbey R J 2012 Correlated intermolecular coupling fluctuations in photosynthetic complexes *J. Chem. Phys.* **136** 55102
[15] Schwarzer E and Haken H 1972 The moments of the coupled coherent and incoherent motion of excitons *Phys. Lett.* A **42** 317–8
[16] Haken H and Strobl G 1973 An exactly solvable model for coherent and incoherent exciton motion *Z. Phys.* **262** 135–48
[17] Huo P and Coker D F 2012 Influence of environment induced correlated fluctuations in electronic coupling on coherent excitation energy transfer dynamics in model photosynthetic systems *J. Chem. Phys.* **136** 115102
[18] Huo P and Coker D F 2011 Communication: Partial linearized density matrix dynamics for dissipative, non-adiabatic quantum evolution *J. Chem. Phys.* **135** 201101
[19] Hwang-Fu Y H, Chen W and Cheng Y C 2015 A coherent modified Redfield theory for excitation energy transfer in molecular aggregates *Chem. Phys.* **447** 46–53
[20] Roden J J J, Bennett D I G and Whaley K B 2016 Long-range energy transport in photosystem II *J. Chem. Phys.* **144** 245101
[21] Liu X and Kühn O 2016 Vibrational and vibronic coherences in the dynamics of the {FMO} complex *Chem. Phys.* **481** 272–80
[22] Curutchet C, Kongsted J, Munoz-Losa A, Hossein-Nejad H, Scholes G D and Mennucci B 2011 Photosynthetic light-harvesting is tuned by the heterogeneous polarizable environment of the protein *J. Am. Chem. Soc.* **133** 3078–84
[23] Doust A B, Marai C N J, Harrop S J, Wilk K E, Curmi P M G and Scholes G D 2004 Developing a structure-function model for the cryptophyte phycoerythrin 545 using ultrahigh resolution crystallography and ultrafast laser spectroscopy *J. Mol. Biol.* **344** 135–53
[24] Doust A B, Wilk K E, Curmi P M G and Scholes G D 2006 The photophysics of cryptophyte light-harvesting *J. Photochem. Photobiol.* A **184** 1–17
[25] Novoderezhkin V I, Doust A B, Curutchet C, Scholes G D and Van Grondelle R 2010 Excitation dynamics in phycoerythrin 545: modeling of steady- state spectra and transient absorption with modified redfield theory *Biophys. J.* **99** 344–52
[26] Viani L, Corbella M, Curutchet C, O'Reilly E J, Olaya-Castro A and Mennucci B 2014 Molecular basis of the exciton-phonon interactions in the PE545 light-harvesting complex *Phys. Chem. Chem. Phys.* **16** 16302–11
[27] Misra B and Sudarshan E C G 1977 The Zeno's paradox in quantum theory *J. Math. Phys.* **18** 756–63
[28] Iubini S, Boada O, Omar Y and Piazza F 2015 Transport of quantum excitations coupled to spatially extended nonlinear many-body systems *New J. Phys.* **17** 113030
[29] Scheer H and Zhao K H 2008 Biliprotein maturation: the chromophore attachment *Mol. Microbiol.* **68** 263–76
[30] Mukamel S 1995 *Principles of Nonlinear Optical Spectroscopy* (New York: Oxford University Press)
[31] Curutchet C, Munoz-Losa A, Monti S, Kongsted J, Scholes G D and Mennucci B 2009 Electronic energy transfer in condensed phase studied by a polarizable QM/MM model *J. Chem. Theory Comput.* **5** 1838–48
[32] Zerner M C 1991 Semiempirical molecular orbital methods *Rev. Comput. Chem.* **2** 313–65
[33] Olbrich C, Strümpfer J, Schulten K and Kleinekathöfer U 2011 Theory and simulation of the environmental effects on FMO electronic transitions *J. Phys. Chem. Lett.* **2** 1771–6
[34] Olbrich C, Strümpfer J, Schulten K and Kleinekathöfer U 2011 The quest for spatially correlated fluctuations in the FMO light-harvesting complex *J. Phys. Chem.* B **115** 758
[35] Viani L, Curutchet C and Mennucci B 2013 Spatial and electronic correlations in the PE545 light-harvesting complex *J. Phys. Chem. Lett.* **4** 372–7
[36] Troisi A 2011 Charge transport in high mobility molecular semiconductors: classical models and new theories *Chem. Soc. Rev.* **40** 2347–58
[37] Troisi A and Orlandi G 2006 Charge-transport regime of crystalline organic semiconductors: diffusion limited by thermal off-diagonal electronic disorder *Phys. Rev. Lett.* **96** 86601
[38] Aragó J and Troisi A 2015 Dynamics of the excitonic coupling in organic crystals *Phys. Rev. Lett.* **114** 26402
[39] Kumar S, Tsai C J and Nussinov R 2003 Temperature range of thermodynamic stability for the native state of reversible two-state proteins *Biochemistry* **42** 4864–73
[40] Moix J M, Khasin M and Cao J 2013 Coherent quantum transport in disordered systems: I. The influence of dephasing on the transport properties and absorption spectra on one-dimensional systems *New J. Phys.* **15** 085010
[41] Sisto A, Stross C, van der Kamp M W, O'Connor M, McIntosh-Smith S, Johnson G T, Hohenstein E G, Manby F R, Glowacki D R and Martinez T J 2017 Atomistic non-adiabatic dynamics of the LH2 complex with a GPU-accelerated *ab initio* exciton model *Phys. Chem. Chem. Phys.* **19** 14924–36
[42] Schütze J, Brüggemann B, Renger T and May V 2002 Theory of linear absorption spectra of biological and non-biological chromophore complexes *Chem. Phys.* **275** 333–54
[43] Meier T, Chernyak V and Mukamel S 1997 Femtosecond photon echoes in molecular aggregates *J. Chem. Phys.* **107** 8759–80
[44] Atilgan A, Durell S, Jernigan R, Demirel M, Keskin O and Bahar I 2001 Anisotropy of fluctuation dynamics of proteins with an elastic network model *Biophys. J.* **80** 505–15
[45] Hinsen K, Petrescu A J, Dellerue S, Bellissent-Funel M C and Kneller G R 2000 Harmonicity in slow protein dynamics *Chem. Phys.* **261** 25–37
[46] Micheletti C, Lattanzi G and Maritan A 2002 Elastic properties of proteins: insight on the folding process and evolutionary selection of native structures *J. Mol. Biol.* **321** 909–21
[47] Tama F, Wriggers W and Brooks C L III 2002 Exploring global distortions of biological macromolecules and assemblies from low-resolution structural information and elastic network theory *J. Mol. Biol.* **321** 297–305
[48] Tirion M M 1996 Low-amplitude elastic motions in proteins from a single-parameter atomic analysis *Phys. Rev. Lett.* **77** 1905–8
[49] Bahar I, Lezon T R, Yang L W and Eyal E 2010 Global dynamics of proteins: bridging between structure and function *Annu. Rev. Biophys.* **39** 23–42
[50] Juanico B, Sanejouand Y H, Piazza F and De Los Rios P 2007 Discrete breathers in nonlinear network models of proteins *Phys. Rev. Lett.* **99** 238104
[51] Sanejouand Y H 2013 Elastic network models: theoretical and empirical foundations (*Biomolecular Simulations*) ed L Monticelli and E Salonen (Berlin: Springer) pp 601–16
[52] May V and Kühn O 2011 *Charge and Energy Transfer Dynamics in Molecular Systems* (New York: Wiley)
[53] Morgan S E, Cole D J, Chin A W, Austin R H and Jansen T L C 2016 Nonlinear network model analysis of vibrational energy transfer and localisation in the Fenna–Matthews–Olson complex *Sci. Rep.* **6** 36703